INVESTIGATION OF CLEAVAGE FRACTURE UNDER DYNAMIC LOADING CONDITIONS: PART I FRACTOGRAPHIC ANALYSIS

Johannes Tlatlik

Fraunhofer Institute for Mechanics of Materials IWM, Wöhlerstr. 11, 79108 Freiburg, Germany

johannes.tlatlik@iwm.fraunhofer.de

Abstract

The fracture toughness of ferritic steels under dynamic loading conditions on the one hand shows decreasing values with elevated loading rates but on the other hand the shape of the temperature dependent fracture toughness curve has turned out to be different from the static Master Curve according to ASTM E 1921. This difference is often explained by adiabatic heating in the crack tip region, yet it is not clear if there are other additional mechanisms under dynamic loading conditions that contribute to these changes. This work is dedicated to systematically identifying and quantifying additional mechanisms regarding cleavage fracture under dynamic loading conditions. In part I of this study an extensive fractographic analysis of the fracture surfaces was conducted for various crack tip loading rates and testing temperatures. The primary fracture-inducing mechanism was found to be identical to the dominant one under quasi-static conditions (carbide cracking). Yet, the dynamic loading conditions appear to change the origin of fracture, promote local crack arrest, and cause multiple fracture initiation sites that lead to global failure. These results also question the reliability of current local approach concepts if used to assess fracture probability at elevated loading rates. The fractographic results are used in, and complemented by, part II of this study which deals with the numerical analysis of other additional mechanisms such as inertia.

Key Words

Dynamic Fracture Mechanics, Cleavage Fracture, Fractography, Master Curve Concept, Crack Arrest

Nomenclature

a_0	initial crack length
h	local stress triaxiality
K_I	stress intensity factor
K_{Ic}	fracture toughness
K_{Icd}	dynamic fracture toughness (elastic)
K_{IR}	ASME lower boundary curve
K_J	stress intensity factor (small scale yielding)

$K_{J,1T}$	size corrected stress intensity factor (small scale yielding)
K_{Jcd}	dynamic fracture toughness
$K_{Jcd,1T}$	size corrected dynamic fracture toughness
$K_{Jcd,1T\_50\%}$	median fracture toughness curve with 50 % failure probability
x_{cl}	distance of origin of fracture from crack tip
T_0	Master Curve reference temperature
W	specimen height
ε_e^{pl}	accumulated plastic equivalent strain
$d\varepsilon/dt$	strain rate
σ_I	maximum principal stress
ASME	American Society of Mechanical Engineers
DCG	ductile crack growth
IWM	Fraunhofer Institute for Mechanics of Materials IWM
MC	Master Curve
SE(B)	single edge-notched (bending)

1 Introduction

Brittle failure must be compellingly ruled out in safety-relevant nuclear components such as reactor pressure vessels. The failure of these ferritic-bainitic steels is usually conducted by macroscopic assessment methods in a deterministic or probabilistic manner. Examples for deterministic concepts are given by the ASME-Codes [1] [2] [3], while the prominent method in terms of a probabilistic assessment is known as the Master Curve (MC) concept, standardized in ASTM E 1921 [4]. Deterministic concepts assume non-failure if a load parameter like the stress intensity factor K_I remains below a certain material-specific value, i.e. critical fracture toughness K_{Ic}, under dynamic conditions referred to as dynamic fracture toughness K_{Icd}. However, the great practicality and simplicity of this method is confronted with widespread experimental results showing that brittle failure is always associated with a large scatter in results, which is explained by the statistical distribution of potentially cleavage-inducing brittle particles within the material (Chen et al. [5]). In this context, macroscopic probabilistic methods such as the MC concept have improved cleavage fracture assessment meaningfully, due to the fact that they respect the nature of cleavage fracture by assessing a probability of failure. This concept solely uses the obtained experimental fracture toughness values, and describes a material's temperature-dependent probability towards brittle failure by using a statistical formalism. It assumes a similar progression of all curves for all ferritc-bainitic materials and their conditions, whereas a sole parameter T_0 (MC reference temperature) can be used to classify a materials resistance towards brittle failure. T_0 is defined as the temperature at which the median fracture toughness curve $K_{Jcd,1T\_50\%}$ has a fracture toughness of 100 MPa√m. Moreover, more brittle material conditions coincide with a MC shifted towards higher temperatures, and vice versa (more information available in ASTM E 1921 [4]).

Since the reactor catastrophe in Fukushima in 2011 the German competence pool for nuclear technology is especially concerned with the safety assessment of nuclear components subjected to explosions, air plane crashes, earth quakes, etc. [6]. In connection with falling debris onto the reactor pressure vessel the material's behavior at elevated loading rates must be understood and characterized. Eventually, the MC concept is technically allowed to be used to assess brittle failure at elevated loading rates, or in other words dynamic loading conditions. However, recent experimental data from various sources states that the achieved dynamic fracture toughness values K_{Jcd} do not match the calculated shape of the MC, especially for higher temperatures or higher dynamic fracture toughness values. An example of this is shown in Figure 1 from Reichert et al. [7], while very similar observations have been made by Mayer et al. [8] or Böhme et al. [9]. Figure 1 shows fracture toughness values of three test series at -20, 0, and +20 °C at an elevated crack tip loading rate of $4{\cdot}10^5$ MPa√m/s (rather fast), whereas the dynamic embrittlement, represented by the T_0-shift from quasi-static conditions, is correctly conceived by the MC concept. The dashed line indicates the calculated median facture toughness $K_{Jcd,1T\_50\%}$ for all test series together (multi-temperature method), while reference temperatures for the three individual test series are depicted next to the fracture points with the experimental median value (large white diamonds). It is apparent that the multi-temperature method does not match the experimental results, and that the individual T_0-reference temperatures are very different from the one obtained by the multi-temperature method (-10 °C). Noteworthy at this point is that the test series with lower fracture toughness values at -20 °C does not necessarily produce lower values than expected, but that the median $K_{Jcd,1T\_50\%}$ curve is constructed from all test series, being a best fit for the entire temperature range.

The mentioned discrepancies are often explained by the presence of adiabatic heating at the crack tip due to the short testing times (Zehnder and Rosakis [10]). Schindler and Kalkhof [11] proposed an adjustment of the MC concept by changing the exponent that controls the shape of the curve, which has been pursued and adapted by Reichert et al. [7], Mayer et al. [8], and Böhme et al. [9], unitarily proving this procedure to be accurate. Furthermore, these discrepancies are also observed for rather slow crack tip loading rates of $4{\cdot}10^3$ MPa√m/s (Reichert et al. [7]), which only correspond to a nominal test velocity of about 0.025 m/s for the specific specimen geometry used in Reichert et al. [7] (SE(B)40-20).

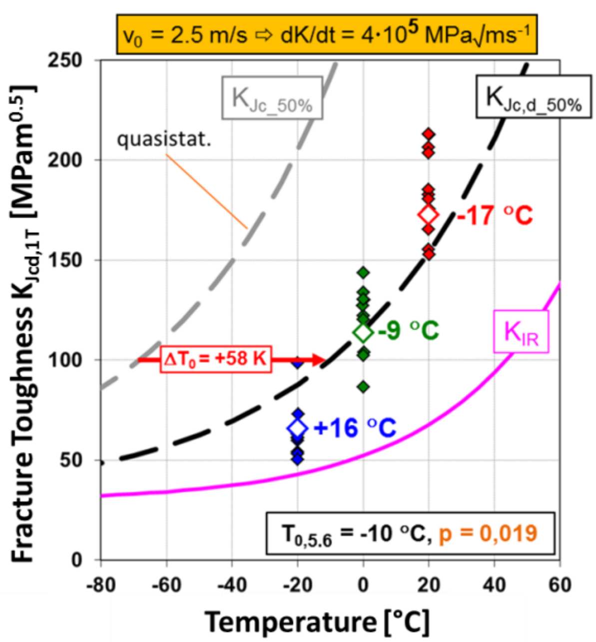

Figure 1: Median Master Curve $K_{Jcd,1T\_50\%}$ (multi-temperature method). Colored symbols are the individual fracture toughness values, and white icons the median values. Displayed is also the quasi-static Master Curve for the material and the ASME lower boundary curve K_{IR} (Reichert et al. [6]).

On the other hand, there exist more complex *local* probabilistic methods to assess cleavage fracture, also known as *local approach*, which numerically calculate global failure of a structure or specimen by direct assessment of local mechanical field values (stresses and strains) in the vicinity of the crack tip. In other words, probability of cleavage fracture is assessed by consideration of real micromechanical processes at the origin of cleavage initiation. Some examples of these local approaches are published by Beremin et al. [12], Faleskog et al. [13], or more recently by Hohe et al. [14], all with similar backgrounds, yet the levels of complexity vary. For ferritic-bainitic steels in the brittle-ductile transition area literature (Knott [15], or McMahon et al. [16], Griffith [17]) generally agrees on the fact that cleavage fracture is mainly caused by the following scenario:

1. Brittle carbides at grain boundaries break causing microdefect evolution.
2. Subsequently, the freshly nucleated crack can become instable and propagate.
3. Assuming the crack propagates a certain distance (usually one grain) and does not blunt, definite failure of the structure is assumed (weakest link concept Mudry [18]).

This is implemented by local approach models, such as the one developed by Hohe et al. [14], by analyzing the local development of the mechanical field variables: accumulated plastic equivalent strain ε_e^{pl}, local stress triaxiality *h*, and maximum principal stress σ_I. Cleavage fracture probability is ultimately calculated through a complex interaction of these variables. Like presented in Figure 4, it is assumed that higher levels of accumulated plastic equivalent strain ε_e^{pl} increase the probability of defect evolution, while local stress triaxiality *h* controls whether or not a fresh crack remains sharp or blunts. Finally, instable crack propagation is initiated when maximum principal stress σ_I reaches a critical value, depending on the size of the evolved defect. The probabilistic character is implemented by considering the size distribution of the brittle particles/carbides within the ferritic matrix.

The assumption of this scenario, and the implementation of the variables (in various levels of complexity), are the basis of all of the mentioned local approaches, and the agreement with experiments under quasi-static conditions is good. However, it is not clear if the mentioned scenario is appropriate under dynamic loading conditions as well, which in turn would question the applicability of these models to dynamic loading conditions (like the MC concept).

This study is dedicated to identifying the relevance of additional mechanisms that influence fracture behavior under dynamic loading for both of the mentioned assessment types. Under dynamic loading conditions, the following additional mechanisms are thought to potentially have impact on the fracture behavior:

1. temperature increase,
2. strain rate increase,
3. wave phenomena,
4. crack arrest,
5. other fracture-inducing mechanisms (i.e. different particle types),
6. local temperature increase at the particle-matrix interface.

Due to the lack of physical background, all of the mentioned mechanisms potentially impact the MC concept, yet their relevance is not clear. Assuming the use of adequate temperature- and strain rate dependent material properties, as well as dynamic simulation conditions, local approach concepts would inherently conceive the first three, because the resulting mechanical field variables would change according to these adaptations as well. However, the relevance of mechanisms 4-6 would severely change the physical fundament of these local approaches under elevated loading rates, so that an adjustment would be necessary.

For this study a combined fractographic and numerical approach is used to identify the relevance of the six mechanisms under dynamic loading, whereas part I only covers the fractographic analysis. Fractography is used to identify the relevance of mechanism 4 and 5, whereas it is also used to determine the exact origin of cleavage fracture for every specimen. Part II is aided by origin of fracture, and then discusses the other mechanisms via a numerical approach.

The basis for this is a large experimental database involving dynamic fracture mechanics of SE(B)40-20 ($a_0/W \approx 0.32$ on average) experiments for several elevated crack tip loading rates of 10^3, 10^4, and 10^5 MPa√m/s at temperatures of -20, 0, and +20 °C which was developed previously in other studies at Fraunhofer IWM. The test series include 8-12 specimens, and the striker velocity of the servo-hydraulic testing machine was in the region of 0.025-2.5 m/s. The examined material is a German reactor pressure vessel steel 22 NiMoCr 3-7, and the dimensions of the specimen can be seen in Figure 2. All tests and evaluations were based on ASTM E 1921 [4], including the fatigue pre-cracking procedure. The range of applicability was extended to higher loading rates and fracture times partially less than 100 µs by the usage and development of special measuring techniques (i.e. near crack tip strain gauges). Detailed information on the actual testing can be found in Böhme et al. [19], whereas some background can be seen in Figure 3 from the mentioned reference.

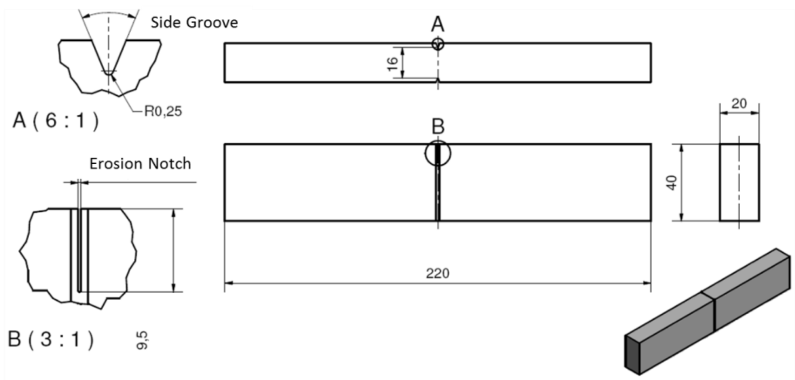

Figure 2: Dimensions of the used bending specimen SE(B)40-20.

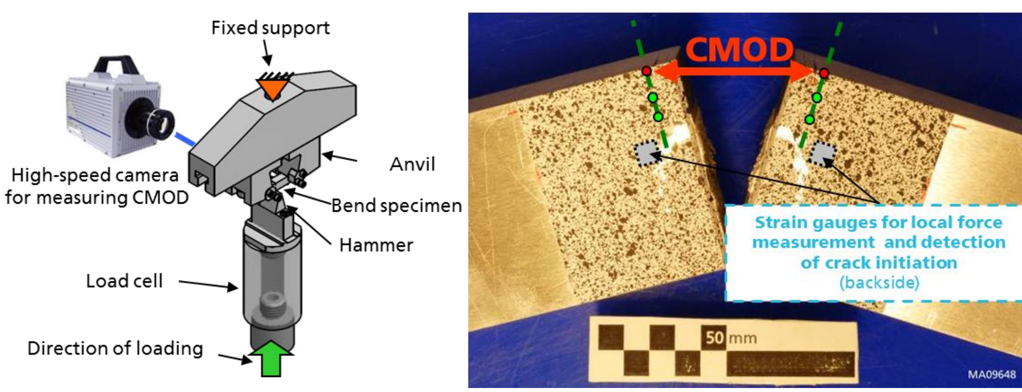

Figure 3: Test set-up used for the dynamic fracture mechanics tests, and measurement of CMOD with digital image correlation as reported by Böhme et al. [19].

At this point a color- and symbol-coding is introduced to distinguish between different test temperatures and crack tip loading rates. Various shades of blue, green and red represent the different testing temperatures of -20, 0, and +20 °C, respectively. An increase in number of corners regarding the symbol types ranging from circle, over triangle, to square, represent the increase in crack tip loading rate from 10^3 to 10^4 to 10^5 MPa√m/s. In addition, and only relevant for the fractographic examinations, a red "X" displays very high crack tip loading rates of 10^6 MPa√m/s at +20 °C. Also, all dynamic fracture toughness values are size-corrected according to ASTM E 1921 [4] (1T) to $K_{Jcd,1T}$ with

$$K_{Jcd,1T} = 20 + (K_{Jcd} - 20)\left(\frac{B}{25}\right)^{1/4} \tag{1}$$

whereas B represents the specimen thickness without side grooves. No constraint correction was applied to the dataset.

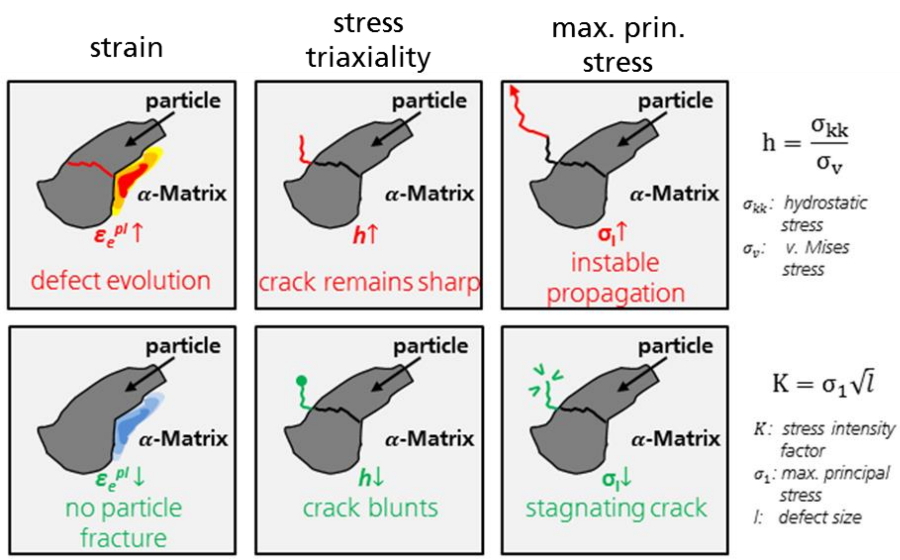

Figure 4: Principal or schematic influence of the mechanical field variables accumulated plastic equivalent strain ε_e^{pl}, local stress triaxiality h, and maximum principal stress σ_I on the cleavage fracture mechanism in the brittle-ductile transition area.

2 Fractographic Examinations

2.1 Origin of Cleavage Fracture Initiation

The knowledge of the exact location or origin of cleavage fracture is of vital importance for local concepts, because the cleavage-controlling mechanical field variables are location-dependent. A typical identification of the origin of cleavage fracture with the aid of scanning electron microscopy is shown in

Figure 5. The radiating fracture patterns are followed to the origin by increasing magnification like proposed by Bouchet et al. [20]. The distance of the origin of cleavage fracture from the crack tip – not including the individual ductile crack growth (DCG) – is quantified by the value x_{cl}. Often, a clear origin cannot be determined, upon which a most probable location is chosen with a corresponding uncertainty margin. In some rare cases these uncertainty margins can reach up to ± 200 µm, while in most cases the origin could be narrowed down to an uncertainty of very few micrometers. For this work only primary initiation sites were considered that need to be separated from secondary sites. Primary initiations lead to failure of the complete structure/specimen, and show mainstream fracture patterns on the entire fracture surface (see Figure 5), and are the cause the sudden drop of force regarding fracture mechanics experiments. Secondary initiation sites are incidental, and most likely take place after a primary initiation, having no effect on macroscopic failure (see Figure 6 a) left). As seen, they do not cover a significant fraction of the fracture surface in contrast to the primary initiation sites. However, not only double, but also triple and quadruple primary cleavage fracture initiation sites were registered and treated equally in this study, meaning that a single specimen can have several corresponding fracture origins in the following images. Typical examples of such multiple initiations are shown in Figure 6 b) - d).

The probability of multiple initiations increases strongly for conditions that result in low fracture toughness values. Technically, the multiple initiation sites contradict the weakest link assumption, and therefore the Master Curve concept, yet the agreement of the dynamic MC at lower fracture toughness values is still good, in contrast to higher ones where the discrepancy is high, and multiple sites are uncommon. In conclusion, this topic will not be discussed in-depth, because the relevance of the topic is not clear, yet some examples are shown in Figure 7 to provide some information.

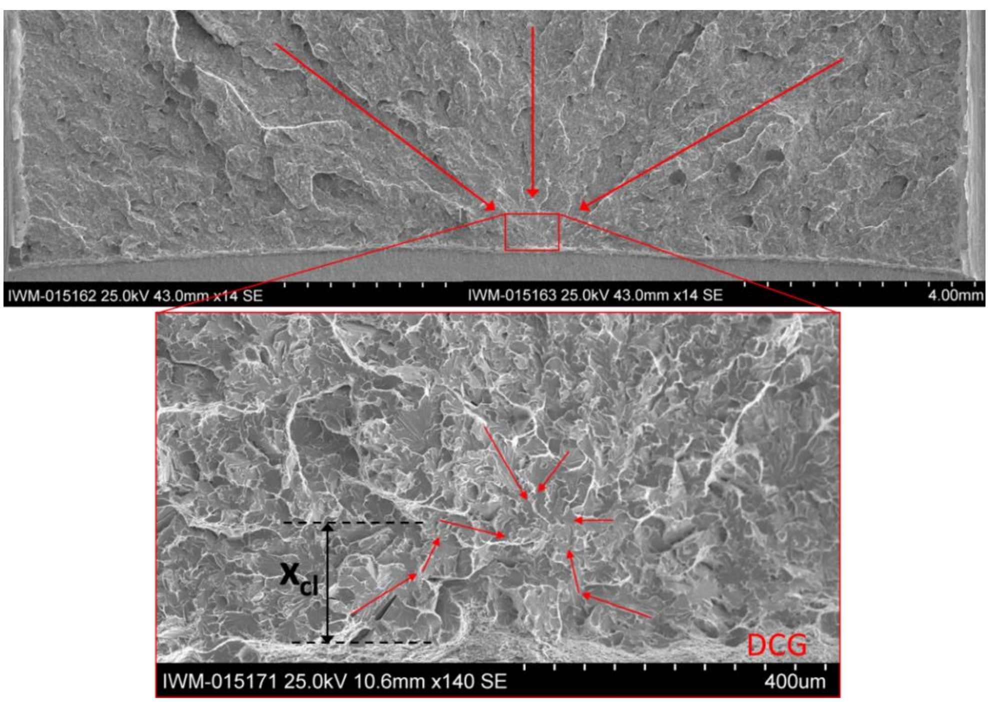

Figure 5: Procedure for locating the origin of cleavage fracture from the individual crack front and the specimen specific ductile crack growth zone (DCG).

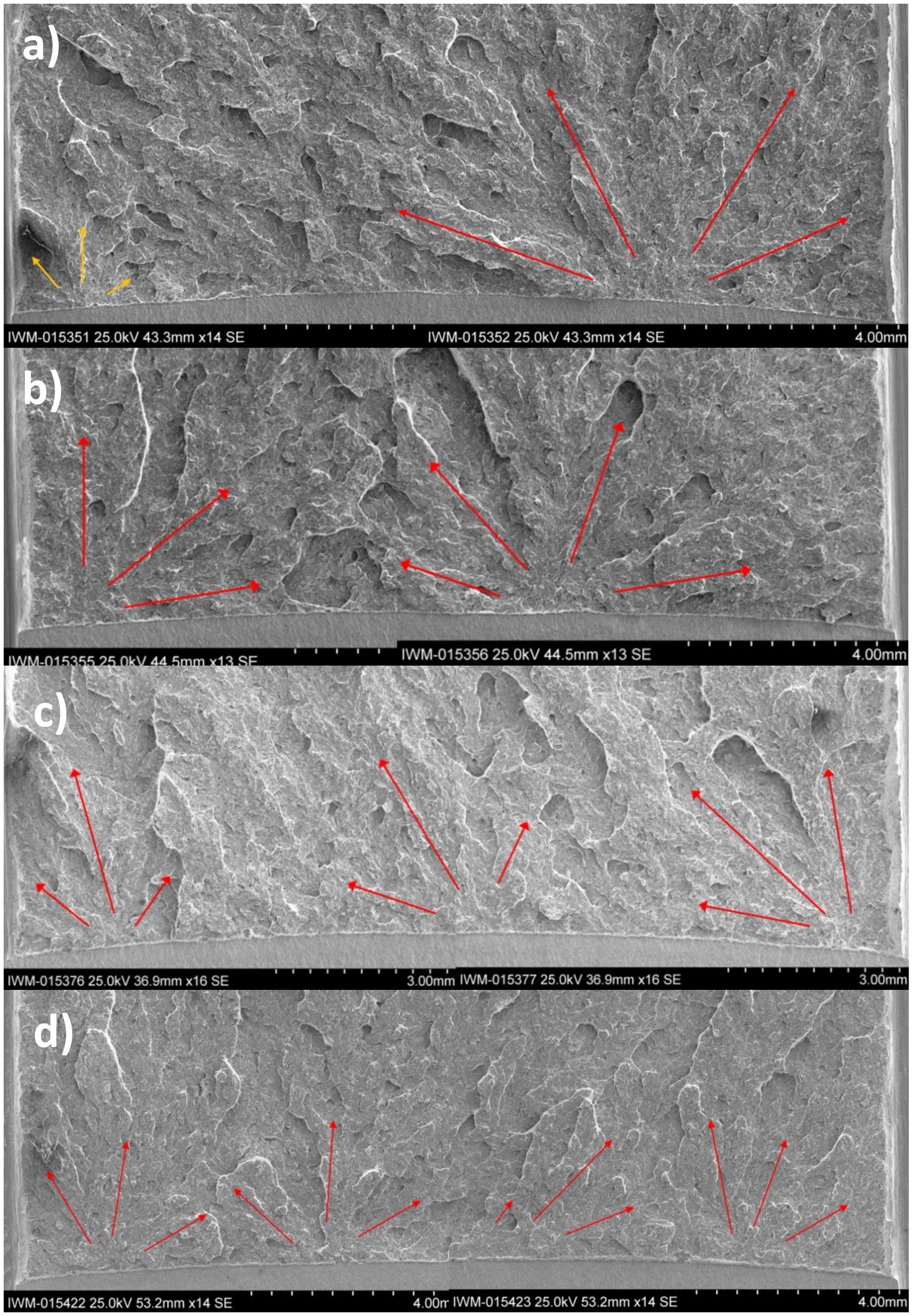

Figure 6: Examples of a) one secondary and one primary initiation; b) two primary initiations; c) three primary initiations; d) four primary initiations

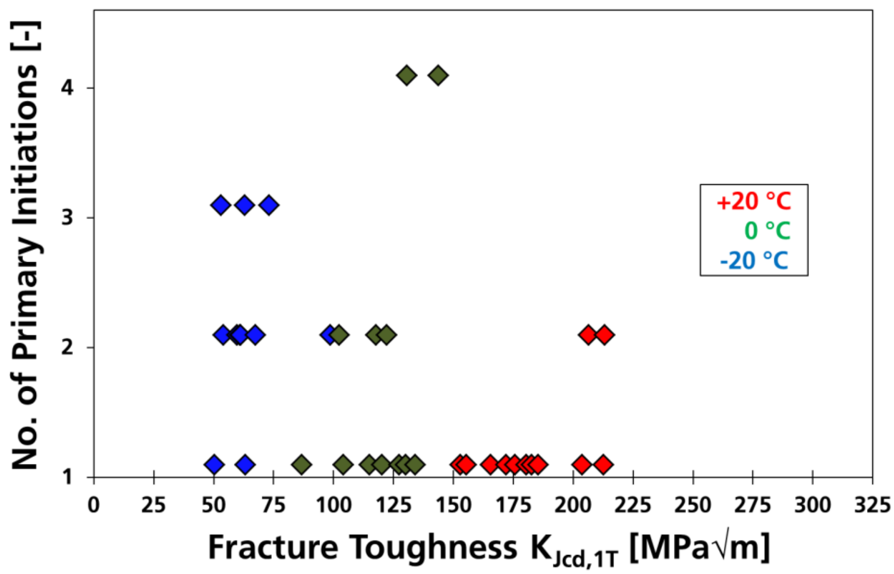

Figure 7: Number of primary initiation sites as a function of fracture toughness for a crack tip loading rate of 10^5 MPa√m/s at different temperatures.

In order to quickly reveal differences compared to quasi-static testing conditions, the scatter band of cleavage location data from work by Hohe et al. [14] was incorporated into Figure 8. It shows the location of fracture as a function of dynamic fracture toughness $K_{Jcd,1T}$. While only observing this quasi-static "funnel" one can see that the location of cleavage generally is found very close to the crack tip for low fracture toughness values. This is connected to the fact that cleavage fracture initiation principally needs some plastic deformation of the matrix to produce a microdefect by stress redistribution around brittle particles, and low crack loads produce very small plastic zones. With increasing crack load the distance of the origin of cleavage fracture also increases. Now, the large plastic zone causes a shift of the peak maximum principal stress, causing microdefect instability, which occurs with increasing load or fracture toughness. Not only does the maximum shift, but it expands to a larger area with more potentially harmful brittle particles that are exposed to sufficiently high stresses. Consequently, a larger scatter is observed towards higher loads.

Introducing symbols in Figure 8, they show the location of cleavage (without ductile crack growth) as a function of fracture toughness for different testing temperatures and different crack tip loading rates (see color- and icon-coding from introduction) under dynamic loading conditions. This also includes multiple initiations at the same fracture toughness which are fairly common at values below 150 MPa√m. It is apparent that very high fracture toughness values of $K_{Jcd,1T} > 225$ MPa√m cause higher distances of the initiation sites, as well as very low values of $K_{Jcd,1T} < 100$ MPa√m. Medium values of $125 < K_{Jcd,1T} < 225$ MPa√m show very similar results compared to the quasi-static data. Noteworthy however, is the fact that very brittle conditions of $K_{Jcd,1T} < 75$ MPa√m are associated with numerous multiple initiations under dynamic conditions. Only considering the single initiations closest to the crack tip the higher distances regarding Figure 3 are moderately redeemed, but slight distances still remain.

Conclusively, the dynamic loading conditions appear to produce certain differences regarding the origin of cleavage fracture which presumably have their roots in the heat generation and distribution, which are in turn influenced by a variation of crack tip loading rate. This becomes very obvious by observing Figure 9. Here, the data from Figure 8 was described by a log-normal distribution so a probability of occurrence is extracted. Noteworthy here is the fact that a log-normal distribution matches all test series very well, as opposed to Weibull distributions that are very commonly used for this description under quasi-static conditions. While considering the mean origin of 50 % of all test series only a very general increase of the origin of fracture with fracture toughness can be observed with strong variations. However, identical crack tip loading rates (identical icons) reveal a strong linear correlation between the origin of fracture from the crack tip and fracture toughness for all examined probabilities. This matches quasi-static investigations (i.e. [14]) where a general linear correlation was observed. Furthermore, the medium crack tip loading rate of $3{\cdot}10^4$ MPa√m/s shows the steepest slope, while low values of $3{\cdot}10^3$ MPa√m/s are associated with the shallowest. The steeper slope can be explained by the most pronounced heat generation in the region relevant for cleavage fracture initiation compared to slow rates ($3{\cdot}10^3$ MPa√m/s), where much heat is conducted to further away regions, and high rates ($3{\cdot}10^5$ MPa√m/s), where much heat is still much closer to the crack tip. This will be further discussed in Part II of this study involving the numerical calculations.

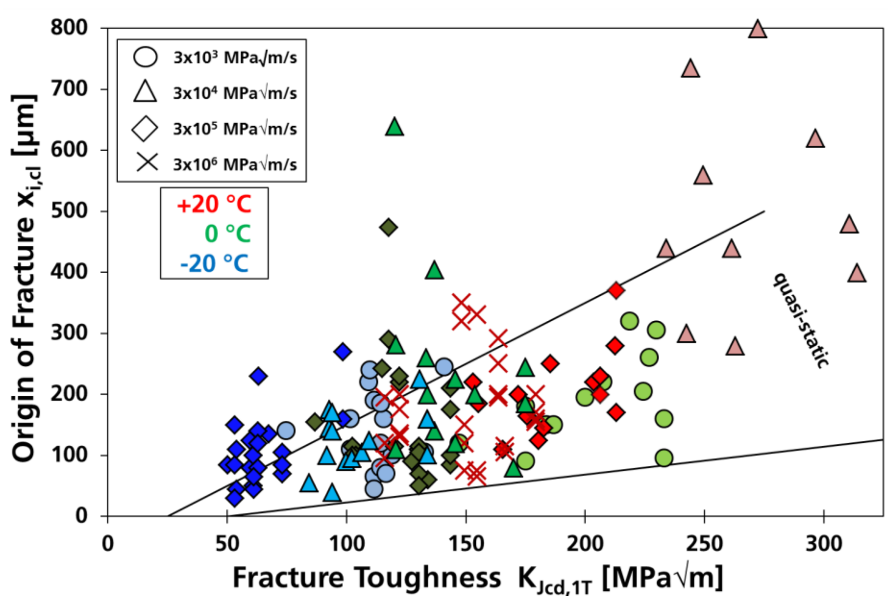

Figure 8: Distance of cleavage initiation from the crack tip (not including ductile crack growth) for the entire database without error margins with quasi-static data (black lines) from [14].

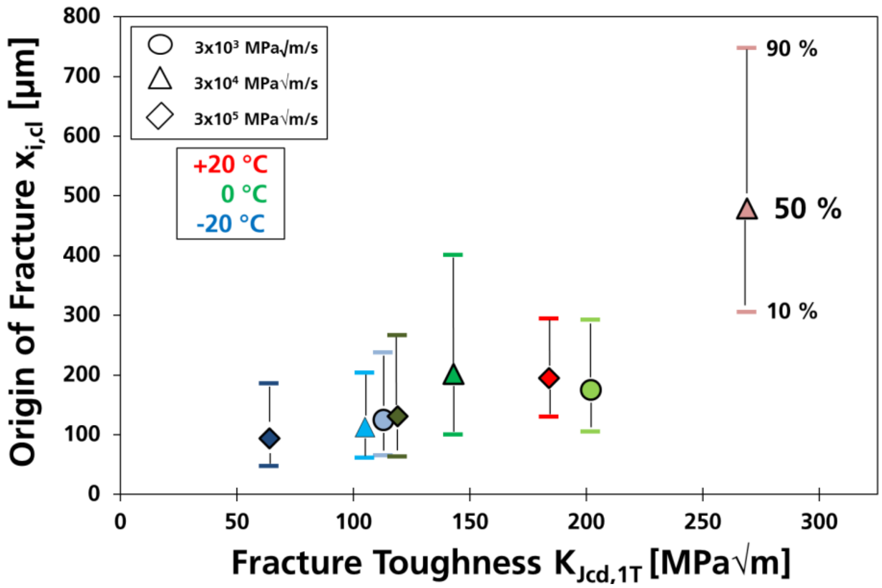

Figure 9: Statistical distribution (log-normal) of the origin of fracture from the crack tip (not including ductile crack growth) for the entire database.

2.2 Fracture-Inducing Mechanisms

Like seen in Figure 10 left, very large manganese sulfide inclusions are observed in the microstructure of this particular material. They are of particular interest for cleavage fracture, because they potentially provide a different physical background of the fracture initiation mechanism than carbides. This was suggested by i.e. Böhme et al. [9] who suspected a possible second initiation mechanism like this due to differences in the statistical data obtained from dynamic fracture mechanics experiments. From a physical standpoint this can be connected to the fact that MnS particles are much larger, softer, and possess a very different thermal expansion coefficient than Fe_3C. A detachment rather than fracture is the result which is thoroughly discussed by authors like Brooksbank et al. [16], and exactly the same mechanism is obvious in Figure 10 left regarding this present study. This mechanism has been connected to cleavage fracture by i.e. Tweed und Knott [22] [23], as well as by Tanguy et al. [24], yet often times the mechanism was only triggered by the usage of Charpy specimens without a precrack. On the one hand, this test has a dynamic character like the ones here, but it produces very large plastic deformations at the crack tip not comparable to actual fracture mechanics experiments. Nevertheless, the strongly changed conditions at the crack tip at elevated loading rates could provoke a shift in the cleavage fracture inducing mechanism, which is discussed below.

In all cases the conventional failure mechanism was identified as transgranular, consistent with observations made by other authors like Hohe et al. [14]. In this present study, examined fracture surfaces only rarely (about 4) showed manganese-sulfide inclusions in the vicinity (100 to 200 µm) of a cleavage fracture initiation location, therefore not showing a clear connection (Figure 10 left). Only in one of these cases could the inclusion be suspected as fracture-inducing, yet there were also three other failure-causing initiation sites along the crack front (multiple initiations), ruling out manganese-sulfide inclusions as a significant cleavage fracture cause under dynamic conditions. Figure 10 right shows this particular origin of fracture, where a rather rare occurrence of a MnS cluster is needed for cleavage fracture.

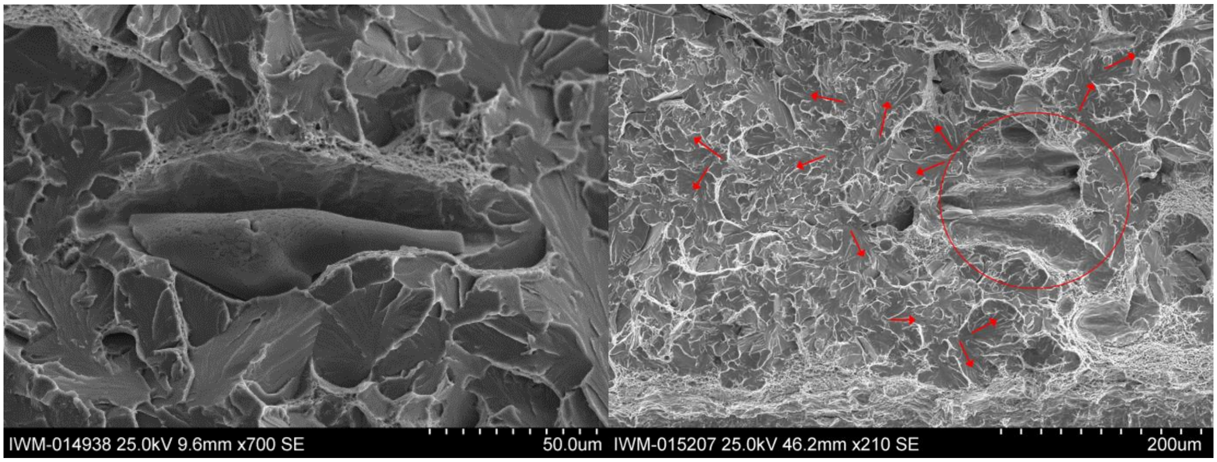

Figure 10: left: Large detatched (not fractured) MnS inclusion found in the vicinity of cleavage initiation; right: MnS cluster that can be seen as cleavage fracture initiation-inducing.

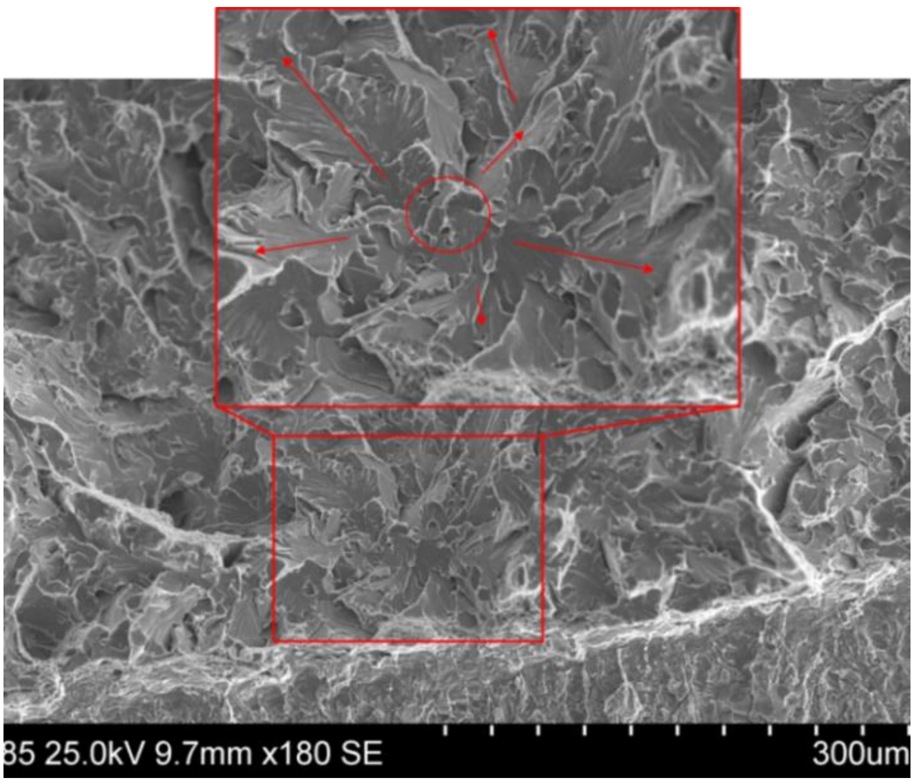

Figure 11: Very typical initiation site at the boundary of (several) grains, most likely carbide-induced.

Aluminum-oxide inclusions (Al_2O_3) were never found in the vicinity of an initiation site (despite the occurrence in the material's microstructure), and also plastic deformations (voids) could not be connected to cleavage fracture initiation either. In principle, clearly locatable initiation sites could be found near (multiple) grain boundaries, most likely being governed by carbides cracking, like seen in Figure 11.

In conclusion, the type of initiation mechanism of cleavage fracture under dynamic loading conditions is assumed to be the same as under quasi-static isothermal conditions. Therefore, mechanism 5 from section 1 is discarded as a meaningful additional mechanism.

2.3 Local Crack Arrest

Fractographic examinations additionally revealed the presence of local crack arrest in the crack tip region. Local crack arrest is only very rarely observed under quasi-static testing conditions, and generally neglected as a meaningful mechanism, yet the topic is still addressed i.e. by Wallin [25]. At higher temperatures initiation toughness and arrest toughness can be similar, therefore influencing the shape of the Master Curve. However, this present study revealed that dynamic loading conditions appear to trigger this mechanism heavily – even for only marginally dynamic conditions of 10^3 MPa√m/s. In terms of fracture assessment, this mechanism is of vital importance because it postpones global failure, leading to higher fracture toughness values. Typical local crack arrest can be seen in Figure 12. They are distinguished by the fact that a clear cleavage initiation occurred, and crack propagation was stopped within the microstructure before global failure. Subsequent load increase most likely caused the stretched zone and significant plastic deformation at the fresh crack tip. An important difference to conventional crack arrest, like discussed in ASTM E 1221-12 [26], is that here observed crack arrest is very local, propagating only about 25 to 300 µm and not several millimeters, yet phenomenologically differing from immediate crack blunting after microdefect evolution upon propagating into the ferritic matrix. A rather large example can be seen in Figure 12 right. This type of local crack arrest is also to be separated from arrest regarding Hopkinson-Bar tests, where a strong stress pulse causes cleavage, and arrest arises due to the sudden loss of crack driving force. Local crack arrest is also to be distinguished from inclusion-induced voids, which can appear similar in geometry, but lack typical river patterns and facets associated with cleavage fracture.

The majority of the local arrest occurrences appeared to be approximately 75 µm in diameter, whereas many can reach up to several hundred µm, and a slight tendency towards larger diameters with increasing fracture toughness values was observed. To introduce the results, Figure 13 is shown that demonstrates the documented number of local arrests on each individual fracture surface for one crack tip loading rate at different temperatures. A general increase of the local arrest probability with an increase in fracture toughness is apparent, and the probability appears to increase within a test series as well. Figure 14 shows the documented number of local arrests on each individual fracture surface for *all* test series. A glance at the image confirms crack arrest under dynamic loading to be highly relevant for all testing conditions, even for the slowest crack tip loading rate that constitutes a striker velocity of only 0.025 m/s, and a test time of about 0.07 s. This loading rate is not associated with conventional dynamically-induced conditions such as inertia or wave phenomena as examined by Böhme [27], and therefore must have a different origin. Most importantly, local crack arrest shows a general and profound correlation with fracture toughness, regardless of the applied crack tip loading rate or testing temperature. The mechanism becomes very frequent around 100 to 125 MPa√m, whereas fracture toughness values of > 200 MPa√m are often associated with at least 10 individual arrest occurrences for this specimen type. Within all individual test series an increase of the probability for arrest is apparent as well, whereas the large scatter is most likely caused by microstructural aspects. This postponement of global failure through local arrest precisely matches the mentioned discrepancies between experiment and MC in Figure 1, because these become more profound with increasing fracture toughness values. Moreover, they are equally prominent for low crack tip loading rates of 10^3 MPa√m/s, as they are for higher ones, which also matches the stated problem in section 1. Also, current local approach concepts lack this physical mechanism, and are questionable in terms of reliable local cleavage fracture assessment at elevated loading rates.

Furthermore, there is no reliable information concerning the exact load at which initiation and arrest occurred, yet only the presented information on the amount and size of the arrest islands. Since the ductile crack growth zone is a function of load, the distance of the arrest islands from the actual crack tip can be much smaller at the point of global failure than it was during the previous arrest event. Not only are stresses and strains variables of the distance and load, but also the temperature increase, so a more precise knowledge of the time and location of initiation and arrest is needed to fully understand the arrest conditions. This is subject of future projects.

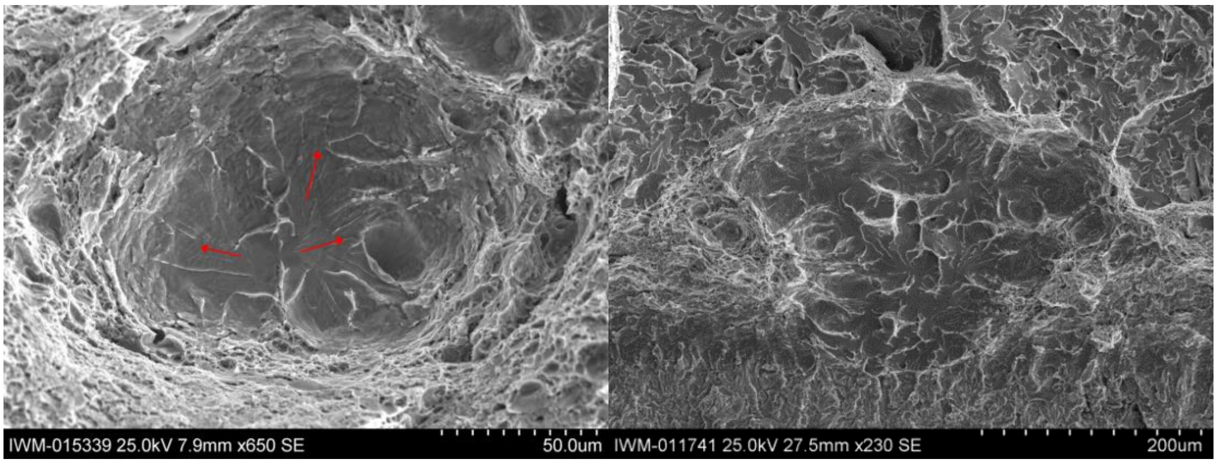

Figure 12: left: Average size arrest occurrence of about 100 µm diameter; right: very large cleavage fracture island of about 250 to 300 µm in diameter.

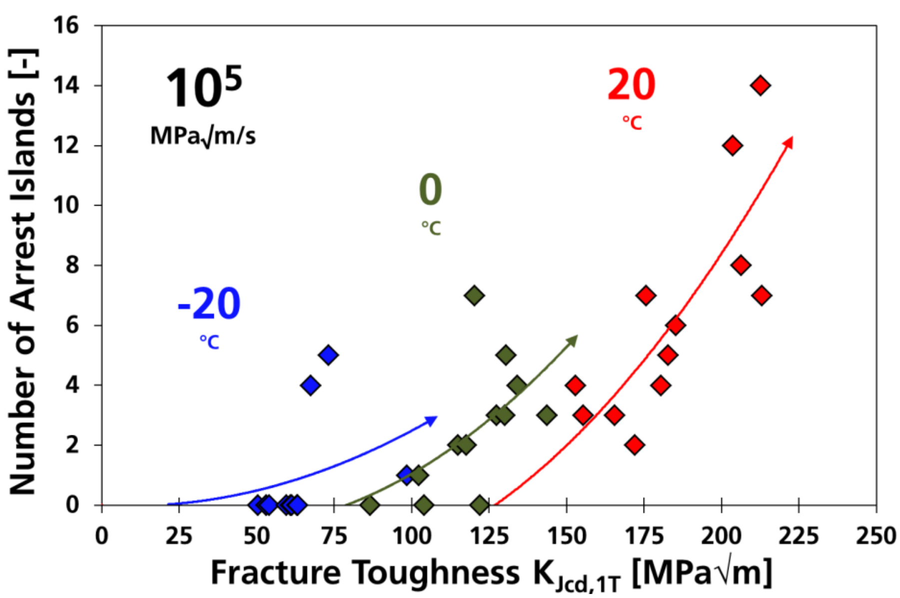

Figure 13: Amount of local arrests per fracture surface as a function of fracture toughness values for a crack tip loading rate of 10^5 MPa√m/s at different temperatures.

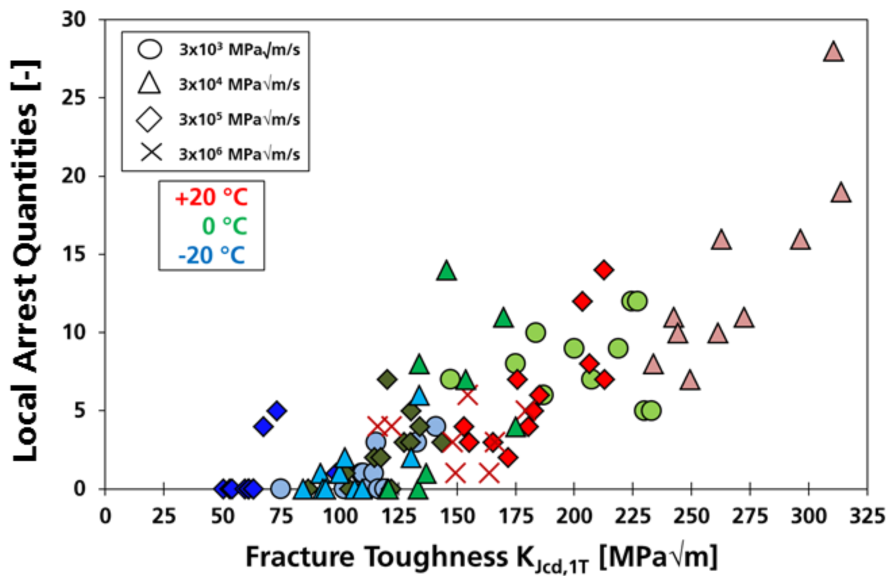

Figure 14: Amount of local arrests per fracture surface as a function of fracture toughness values for all test series.

3 Conclusions

Fractographic investigations of specimens fractured under dynamic testing conditions were thoroughly examined. The primary fracture-inducing mechanism was identified to be linked to carbide-cracking (at grain boundaries), therefore being identical to observations made for quasi-static conditions. Additional fracture-inducing mechanisms are therefore identified as irrelevant. However, the origin of fracture is strongly influenced by these elevated loading rates, and multiple initiations commonly lead to failure for test conditions that are related to low fracture toughness values. The different origins of fracture are most likely linked to the heat generation and conduction in the crack tip region, whereas the data is to be used for numerical simulations in part II of this study that deal with the investigation of the other potentially irrelevant mechanisms. Most importantly, local crack arrest was identified as highly relevant for all dynamic loading situations, and matches the discrepancies between experiments and MC concept. Also, current local approach concepts need to be extended to consider this physical mechanism, and reliably assess fracture probability under dynamic conditions.

Acknowledgement

The investigations were supported by the German Federal Ministry for Economic Affairs and Energy under the support code 1501495 which is thankfully acknowledged by the authors.

References

[1] ASME Boiler and Pressure Vessel Code, Sec. III, Article NB 2300, American Society of Mechanical Engineers, New York 1995.

[2] ASME Boiler and Pressure Vessel Code, Sec. Sec. XI, Article A 3000, Method for KI determination, American Society of Mechanical Engineers, New York 1995.

[3] ASME Boiler and Pressure Vessel Code, Sec. XI, Article A 4000, Material properties, American Society of Mechanical Engineers, New York 1995.

[4] ASTM Standard E 1921-16: Standard test method for determination of reference temperature T0 for ferritic steels in the transition range, ASTM International, West Conshohocken, PA, 2016.

[5] Chen, J.H., Wang, Q., Wang, G.Z., Li, Z.: Fracture behavior at crack tip – a new framework for cleavage mechanism of steel, Acta Mat. 51 (2003) 1841-1855.

[6] Nukleare Sicherheitsforschung, Kompetenzverbund Kerntechnik, Neuorientierung an aktuellen energiepolitischen Rahmenbedingungen, Kap. 4.1.1.2, Mai (2012).

[7] Reichert, T., Böhme, W. and Tlatlik J: Modified Shape of Dynamic Master Curves due to Adiabatic Effects, 21st European Conference on Fracture, ECF21, 20-24 June 2016, Catania, Italy, 2016.

[8] Mayer, U., Reichert, T., Tlatlik, J.: Fracture Mechanics at Elevated Loading Rates in the Ductile to Brittle Transition Region, 2017 ASME Pressure Vessels & Piping Conference, 16-20 2017, Waikoloa, Hawaii, USA, 2017.

[9] Böhme, W., Reichert, T., Mayer, U.: Assessment of dynamic fracture toughness values KJc and reference temperatures T0,x determined for a German RPV steel at elevated loading rates according to ASTM E 1921, SMiRT-22, San Francisco, California, USA, August 18-23, 2013, Division II, Fracture Mech. and Struct. Integrity, 2013.

[10] Zehnder, A.T. und Rosakis, A.J., 1993. Temperature Rise at the Tip of Dynamically Propagating Cracks: Measurements using High Speed Infrared Detectors, J.S. Epstein (Ed.), Experimental Techniques in Fracture, SEM, VCH, New York, pp. 125–169.

[11] Schindler, H. J. and Kalkhof, D.: Lower bounds and saturation effects of dynamic fracture toughness in the brittle-to ductile transition regime of ferritic steels, to be published at 22nd Int. Conf. on Structural Mechanics in Reactor Technology, SMiRT-22, San Francisco, USA, 2013.

[12] Beremin, F.M.: A local criterion for cleavage fracture of a nuclear pressure vessel steel, Metall. Trans. 14A (1983) 2277-2287.

[13] Faleskog, J., Kroon, M. and Öberg, H.: A probabilistic model for cleavage fracture with a length scale – parameter estimation and predictions of stationary crack experiments, Eng. Frac. Mech. 71 (2004) 57-79.

[14] Hohe, J., Hardenacke, V., Luckow, S., Siegele, D.: An enhanced probabilistic model for cleavage fracture assessment accounting for local constraint effects, Eng. Frac. Mech. 77 (2010) 3573-3591.

[15] Knott, J. F.: Micromechanisms of Fracture and the Fracture Toughness of Engineer-ing Alloys. Proc. Of 4th International Conference on Fracture, ICF4 Waterloo, 1977.

[16] McMahon, C.J. and Cohen, M.: Initiation of cleavage in polycrystalline iron, Acta Metall. 13, 591-604, 1965.

[17] Griffith, A.A.: The phenomena of rupture and flow in solids, Phil. Trans. Roy. Soc. London A221 (1921) 163-198.

[18] Mudry, F.: A local approach to cleavage fracture, Nucl. Eng. Des. 105, 65-76, 1987.

[19] Böhme, W., Reichert, T. and Mayer, U., 2013. Assessment of dynamic fracture toughness values KJc and reference temperatures T0,X determined for a German RPV steel at elevated loading rates according to ASTM E1921, 22nd Int. Conf. on Structural Mechanics in Reactor Technology, SMiRT-22, San Francisco, USA, August 18-23, 2013.

[20] Bouchet, G., et al.: Benchmark on the Determination of Cleavage Triggering Sites in a RPV Steel in the DBT Range, International Conference on Fracture 05, Turin, 2005.

[21] Brooksbank, D., Andrews, K.W.: Thermal expansion of some inclusions found in steels and relation to tesselated stresses, Journal of The Iron and Steel Institute, 206:595-599,1968.
[22] Tweed, J.H. and Knott, J.F.: Micromechanics of failure in C-Mn weld metals, Acta Metallurgica 35(7), 1401-1414, 1987.
[23] Tweed, J.H. and Knott, J.F.: Effect of reheating on microstructure and toughness of C-Mn weld metal, Metal Science, 17:45-54, 1983.
[24] Tanguy, B., Besson, J., Piques, R., Pineau, A.: Ductile to brittle transition of an A508 steel characterized by Charpy impact test, part I., experimental results, Engineering Fracture Mechanics, Elsevier, 2005, 72, pp.49-72.
[25] Wallin, K.: The Elusive Temperature Dependence of the Master Curve, 13th International Conference on Fracture, ICF13, 16-21 June 2013, Beijing, China.
[26] ASTM E 1221-12a: Standard Test Method for Determining Plane-Strain Crack-Arrest Fracture Toughness, KIa of Ferritic Steels, ASTM International, American Society for Testing and Materials, West Conshohocken (2012).
[27] Böhme, W.: Experimentelle Untersuchungen dynamischer Effekte beim Kerbschlagbiegeversuch, Dissertation TH Darmstadt.